

Complex magnetic fields in an active region

P.N. Bernasconi¹, C.U. Keller², S.K. Solanki¹, and J.O. Stenflo¹

¹ Institut für Astronomie, ETH-Zentrum, CH-8092 Zürich, Switzerland

² NOAO*/National Solar Observatory, P.O.Box 26732, Tucson, AZ 85726, USA

Received 23 December 1996 / Accepted 22 May 1997

Abstract. High-resolution observations of the full Stokes vector in Fe I spectral lines around 5250 Å obtained at the Swedish Vacuum Solar Telescope on La Palma with the ZIMPOL I Stokes polarimeter in a complex active region reveal the presence of anomalously shaped Stokes profiles indicating the co-existence of at least two magnetic components within the same spatial resolution element. These Stokes profiles have been analyzed with an inversion code based on a 3-component atmospheric model with two magnetic and one field-free component. The fits to the observations in a magnetic region that resembles a small penumbra reveal the presence of a horizontal magnetic field component with an average field strength of $\bar{B} = 840$ G, a mean filling factor of $\bar{\alpha} = 0.12$, and an average temperature $\bar{T} = 5400$ K at $\log \tau_{5000} = -1.5$ embedded in the main “penumbral” magnetic field that has $\bar{B} = 1500$ G, $\bar{\alpha} = 0.56$, and $\bar{T} = 4900$ K. The horizontal component exhibits a mean outflow of 2.7 km s^{-1} which is mainly due to the Evershed flow. In a region where there are strong downflows up to 7 km s^{-1} , we infer the possible presence of a shock front whose height changes along the slit. The height variation can be explained by a change of the gas pressure at the base of the photosphere below the shock front as proposed by Thomas & Montesinos (1991). Small plages with field strengths below 900 G have been observed in the vicinity of some pores. Finally, we present a puzzling field structure at the boundary between two adjacent pores. Ambiguous results suggest that although the inversion code is able to successfully invert even very complex Stokes profiles, we are far from a complete description of the field structure in complex magnetic regions. We warn that magnetograms and fits to data involving only a single magnetic component may hide the true complexity of the magnetic structure in at least some parts of active regions.

Key words: Sun: magnetic fields – flux tubes – active regions – polarimetry

Send offprint requests to: P.N. Bernasconi

* The National Optical Astronomy Observatories are operated by the Association of Universities for Research in Astronomy, Inc., under cooperative agreement with the National Science Foundation.

1. Introduction

Due to seeing and the limited spatial resolution of currently existing solar telescopes, small-scale magnetic features outside sunspots and pores have magnetic and non-magnetic components mixed in one resolution element. The most powerful tool used to overcome this problem is the observation of polarized solar radiation because the polarized profiles (Stokes Q , U , and V) of a Zeeman-split line are only produced by the magnetic component, while the non-magnetic component only contributes to the intensity profiles, i.e. Stokes I .

When measurements are performed in regions with complex magnetic structures, e.g. in sunspot penumbrae or at magnetic neutral lines, more than one magnetic component may be present in the same resolution element. The observed polarized profiles result from the superposition of Stokes signals belonging to different magnetic components and, in particular for Stokes V , they appear distorted as compared with the “normal” profile shapes. Because of the complexity of the Stokes profiles, it is not easy to separate the different magnetic components.

In the infrared, the Zeeman splitting of magnetic lines is larger than in the visible, and the signatures belonging to the different magnetic components are much more evident. For example, Rüedi et al. (1992a, b) successfully analyzed Stokes V profiles of $1.56 \mu\text{m}$ lines showing clear signatures of two magnetic components with different field strengths. Some success has also been obtained in the visible by Skumanich & Lites (1991) and Martínez Pillet et al. (1994), who manually fitted strongly distorted Stokes V profiles in the Fe I 6302.5 Å line with two magnetic components having opposite polarities and different mass motions.

In order to better understand the structure and dynamics of complex magnetic regions, sophisticated inversion codes capable of detecting and separating multiple magnetic components are required. Bernasconi & Solanki (1996) (hereafter referred to as Paper I) have presented an inversion code capable of reproducing anomalously shaped Stokes profiles in terms of a 3-component atmospheric model. In this work we present new results obtained by applying this inversion procedure to Stokes

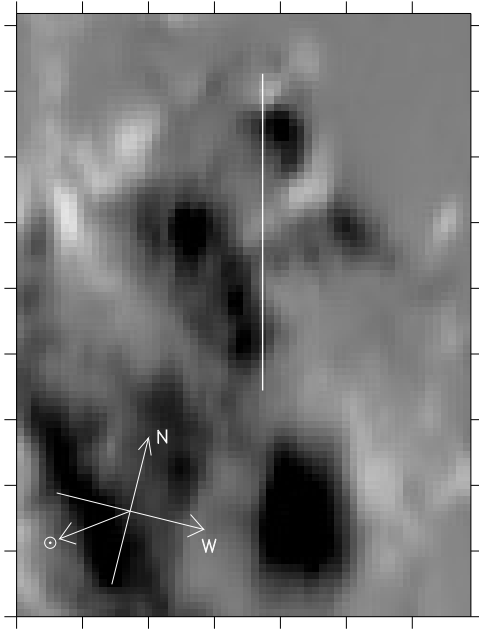


Fig. 1. Detail from the full-disk Kitt Peak magnetogram recorded on May 13, 1993 showing NOAA group No. 7500. The positive polarity fields are represented by the white areas. The vertical line shows the approximate slit position. The tick-mark separation is $10''$. The direction of the heliographic N and W directions and of the disk center are indicated.

profiles of an active region showing a very complex magnetic structure.

2. Observations and data analysis

2.1. Observations and data reduction

The present observations were obtained at the Swedish Vacuum Solar Telescope on La Palma (Canary Islands) on May 13, 1993 with a single camera of the first generation Zürich Imaging Stokes Polarimeter (ZIMPOL I) together with U. Egger, H.P. Povel, and P. Steiner. An overview of the characteristics and capabilities of the polarimeter can be found in Stenflo (1991), Povel et al. (1990, 1994), Keller et al. (1992), and Povel (1995). The complete Stokes vector of the Fe I 5247.1 Å ($g_{\text{eff}} = 2.0$), Fe I 5250.2 Å ($g = 3.0$), and Fe I 5250.7 Å ($g_{\text{eff}} = 1.5$) lines has been recorded in part of NOAA group No. 7500 located at $N 18^\circ$, $W 33^\circ$. The Kitt Peak magnetogram of the group is shown in Fig. 1. The approximate slit position is indicated by the vertical solid line. The angle θ between the normal to the solar surface and the line of sight (LOS) was 40° , which corresponds to $\mu = \cos \theta = 0.76$. A schematic of the optical set-up of the instrument is shown in Fig. 2.

Fig. 3 shows the slit-jaw image recorded with an interference filter centered at 5250 Å as well as the Stokes I , V/I , Q/I , and U/I spectra of the observed active region. The local heliographic coordinate frame and the Sun center direction are indicated in the lower right corner of the slit-jaw image.

The spectrograph slit was $0''.32$ wide and about $50''$ long. We recorded a total of 123 sets of Stokes spectra (I , Q , U , and V) at a single spatial location with a spectral resolving power of 175 000 and a spatial pixel size of $0''.4$. Since, at the time of the observations, only one ZIMPOL I camera was available, we could only record Stokes I plus one other Stokes parameter (Q , U , or V) in a single exposure. The full Stokes vector was then obtained by recording each polarized Stokes parameter in sequence with an integration time of 1 s per measurement and an interval of ~ 150 ms between two consecutive measurements. The sequence of three exposures was repeated seven times, after which the seven images for each Stokes parameter were added together, so that the net integration time per Stokes parameter was 7 s, making it 21 s to record the complete set of Stokes spectra. With this procedure we achieve a sort of quasi-simultaneity in recording all four Stokes parameters with a single CCD camera. We obtain a noise level of 0.25% of the continuum intensity in each Stokes parameter.

We used a spot-tracker system built by C.U. Keller at ETH Zürich to correct image motions due to seeing and telescope guiding errors during the integration (see Fig. 2). During the measurements the quad-cell tracker sensor is pointed at a spot or a big pore located in the vicinity of the observed region. The error signals coming from the tracker are sent to the electronics steering the tilt actuators of the third mirror of the telescope, which keeps the tracked spot or pore in the center of the quad-cell.

The Stokes profiles have been corrected for instrumental polarization by determining the telescope Mueller matrix for the time of the measurement from a theoretical model and applying it to the data (see Paper I; Bernasconi, Fligge & Stenflo, in preparation). After this correction the data are free from instrumental polarization effects to an accuracy of better than 0.5%. The reference system was rotated such that the positive Stokes Q direction is oriented parallel to the geographic $E - W$ direction.

The observed active region shows a complex magnetic structure. Many polarity reversals are visible in the Stokes V image. The Stokes profiles from pixel positions 50 to 60 (see the scale on the right hand side of the Stokes images in Fig. 3) exhibit large Doppler shifts towards the red. More than half of the individual Stokes profiles show clear signatures of at least two magnetic components in the same resolution element. We can subdivide those signatures into three main categories:

1. The Stokes V profiles appear highly distorted relative to the usually antisymmetric shapes and resemble to linear polarization profiles. A typical example is shown in Fig. 4. These profiles belong to a slit position located between two regions with opposite polarities (pixel position No. 46). They can be interpreted as two magnetic components with similar field strengths but with opposite polarities and different flow velocities along the LOS within one resolution element.
2. The Stokes V profiles show a bump or “shoulder” in one or both σ -components. The profiles in Fig. 5 exhibit one “shoulder” in the red wing and a larger Stokes V amplitude for the blue wing. These profiles correspond to pixel po-

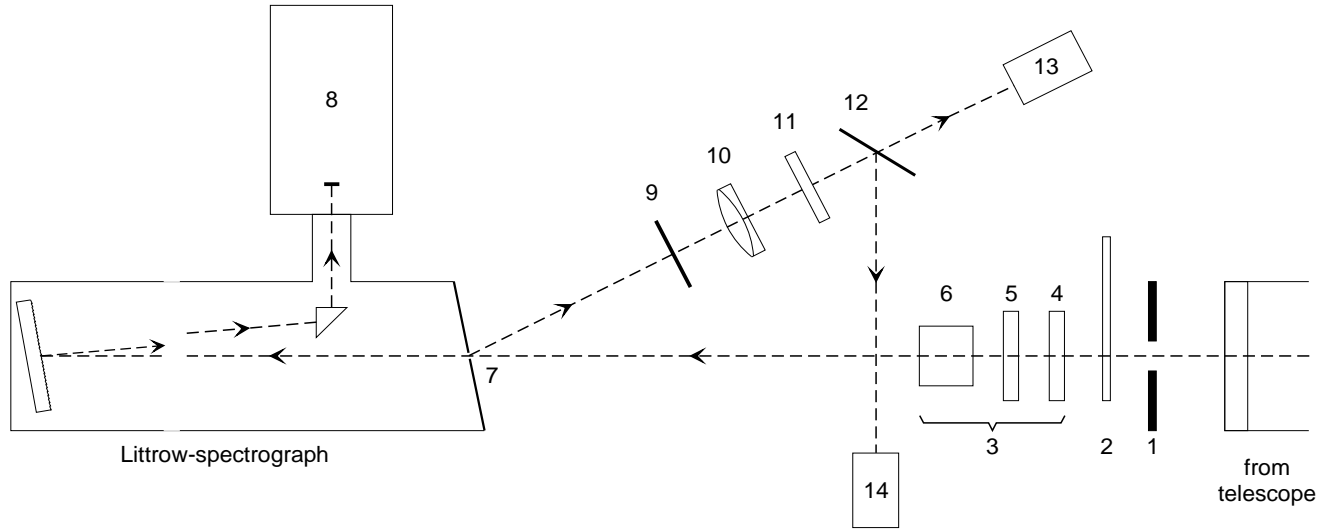


Fig. 2. Schematic of the optical set-up used for the polarimetric measurements performed at the Swedish Vacuum Solar Telescope at La Palma: (1) Circular aperture, (2) filter wheel with polarizers for calibrations, (3) modulator package, (4,5) piezoelectric modulators, (6) Glan polarizer, (7) $32 \mu\text{m}$ reflecting slit, (8) demodulating CCD camera, (9) neutral density filter ND 0.4, (10) 120 mm reimaging lens, (11) green glass filter VG9, (12) 5250 \AA interference filter, 82 \AA bandwidth, (13) COHU CCD video camera, (14) spot tracker sensor.

sition 21 inside a small “penumbra”. In this case the two magnetic components have opposite polarities and different velocities, field strengths, and filling factors. Because of a strong downflow in the weaker component, its Stokes profiles are redshifted with respect to the Stokes profiles of the strong component. This affects especially the red σ -component of the V profiles by producing the shoulder and a reduction of its amplitude.

3. The Stokes V , Q , and U profiles look “normal” but they are Doppler shifted relative to each other as shown in Fig. 6, which corresponds to position 43. Stokes V is redshifted relative to Q and U . This can be explained in terms of two magnetic components having different inclinations with respect to the LOS (one almost parallel and the other almost perpendicular) combined with different velocities.

It is impossible to explain these “complex” profiles by considering a “simple” atmospheric model composed of one magnetic atmosphere embedded in a non-magnetic atmosphere. Therefore we need to carry out multicomponent inversions that we will describe in the following section.

2.2. Inversion of the Stokes profiles

To determine the field strength, field geometry, the temperature stratification, the Doppler shifts, and macroturbulent line broadening from the measured Stokes spectra, we used an inversion code (Solanki et al. 1992, 1994) that fits synthetic Stokes profiles to the observed spectra by using the Levenberg-Marquardt least-squares technique (Press et al. 1990). In Paper I a detailed description of the parts of the inversion code of relevance to multi-component inversions has been given. Here we summarize the most important characteristics of the inversions we have carried out.

To fit “complex” Stokes profiles like the ones shown in Figs. 4, 5, and 6, the inversion code includes the possibility of considering a 3-component atmospheric model. The two magnetic components have different field strengths and geometries as well as different temperature stratifications and velocity fields. The surface fractions covered by the magnetic components in the resolution element are described by the two filling factors α_1 and α_2 . The third component is field-free, i.e. it describes the remaining portion $1 - \alpha_1 - \alpha_2$ of the resolution element, which is only of importance to fit the Stokes I profiles. The resulting synthetic Stokes parameters I_{res} , Q_{res} , U_{res} , and V_{res} are linear combinations of the Stokes parameters emerging from each component weighted by their respective filling factors:

$$\begin{aligned} I_{\text{res}} &= I_1 \alpha_1 + I_2 \alpha_2 + I_3 (1 - \alpha_1 - \alpha_2), \\ Q_{\text{res}} &= Q_1 \alpha_1 + Q_2 \alpha_2, \\ U_{\text{res}} &= U_1 \alpha_1 + U_2 \alpha_2, \\ V_{\text{res}} &= V_1 \alpha_1 + V_2 \alpha_2, \end{aligned} \quad (1)$$

where the subscripts 1 and 2 refer to the two magnetic components and subscript 3 refers to the field-free component, which does not produce any polarization.

For a small number of Stokes profiles it turned out to be impossible to obtain reasonably good fits even by applying a 3-component model atmosphere without introducing additional free parameters. These profiles show very strong asymmetries, in particular in Stokes V where the total area of the positive part of the profiles is very different from the total area of the negative part (see Fig. 7), i.e. they have a large Stokes V area asymmetry. This type of asymmetry cannot be explained by simply considering a multi-component atmosphere. If each single component produces Stokes profiles without area asymmetry, the area asymmetry of the averaged Stokes profiles will also

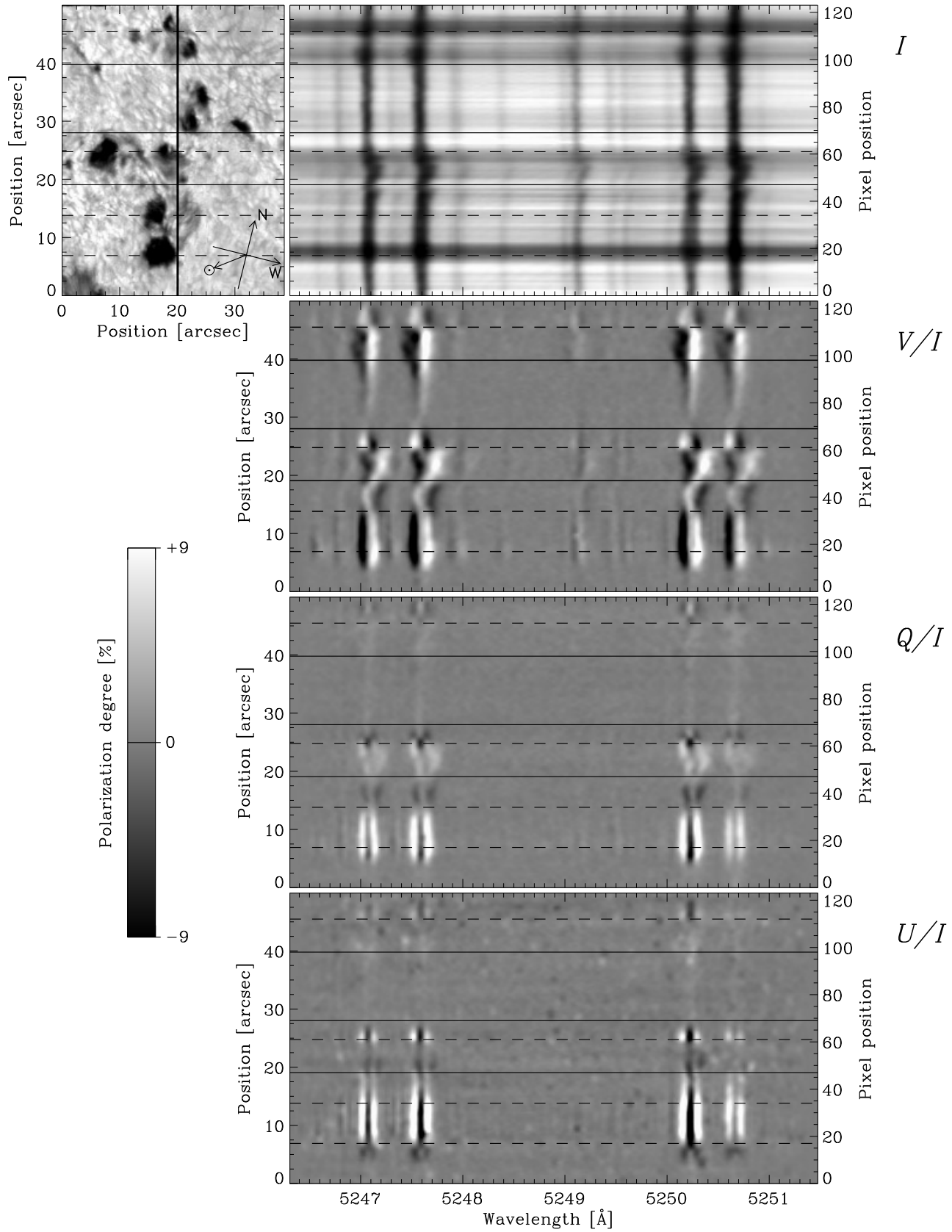


Fig. 3. Slit-jaw and spectral Stokes images of the observed active region. The solid horizontal lines divide the region into four parts that are discussed separately in Sect. 3. The meaning of the dashed lines is discussed in the text.

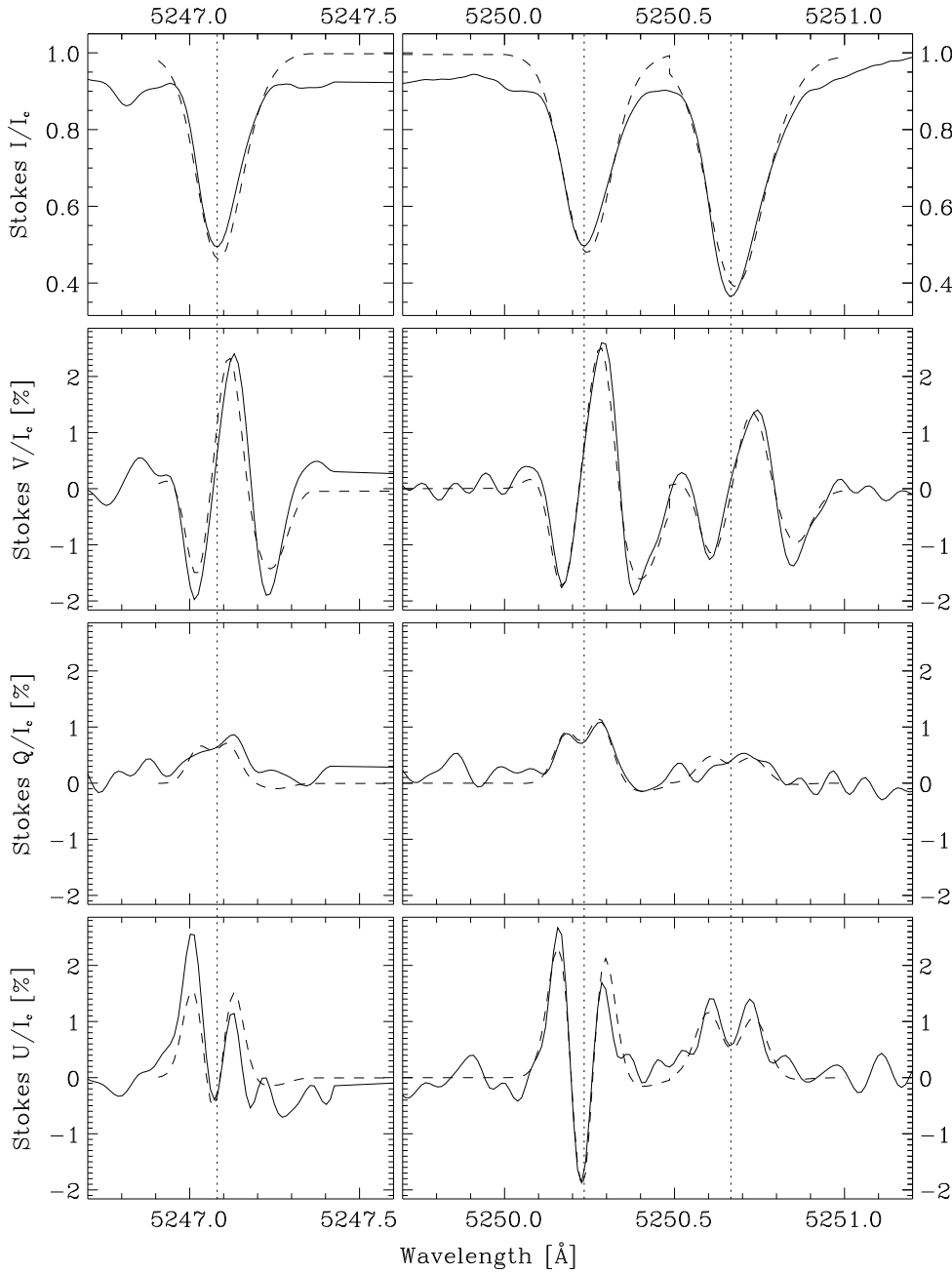


Fig. 4. Observed (solid) and synthetic (dashed) Stokes profiles for pixel position 46. The vertical dotted lines mark the wavelength of the Stokes I minima.

be zero. It is now well established that velocity gradients combined with gradients of the magnetic vector along the LOS are mainly responsible for the observed asymmetries in the Stokes profiles (e.g. Auer & Heasley 1978; Solanki 1989). For this reason we have introduced the velocity and magnetic gradients $\nabla v = \partial v / \partial \log \tau$, $\nabla B = \partial B / \partial \log \tau$ as additional free parameters of the inversion. They are supposed to be independent of optical depth but may be different for the different magnetic components. By combining magnetic and velocity gradients, it is possible to reproduce the shape of the Stokes profiles, even in the case of large Stokes V area asymmetries. An example of such Stokes V profiles is given in Fig. 7.

The model description of the temperature stratification has been discussed in Paper I.

Unlike the fits presented in Paper I the Stokes I profiles have also been included in the fit. Since the magnetic features often provide only a minor contribution to the intensity signal, whereas all of the polarized signals originate in the magnetic regions, we have given a factor of 10 lower weight to the Stokes I profiles. Inclusion of Stokes I gives us better control over the determination of the filling factor, the field strength, and the temperature. Furthermore, the uniqueness of the fits is improved, i.e. the results depend less on the initial guesses for the free parameters.

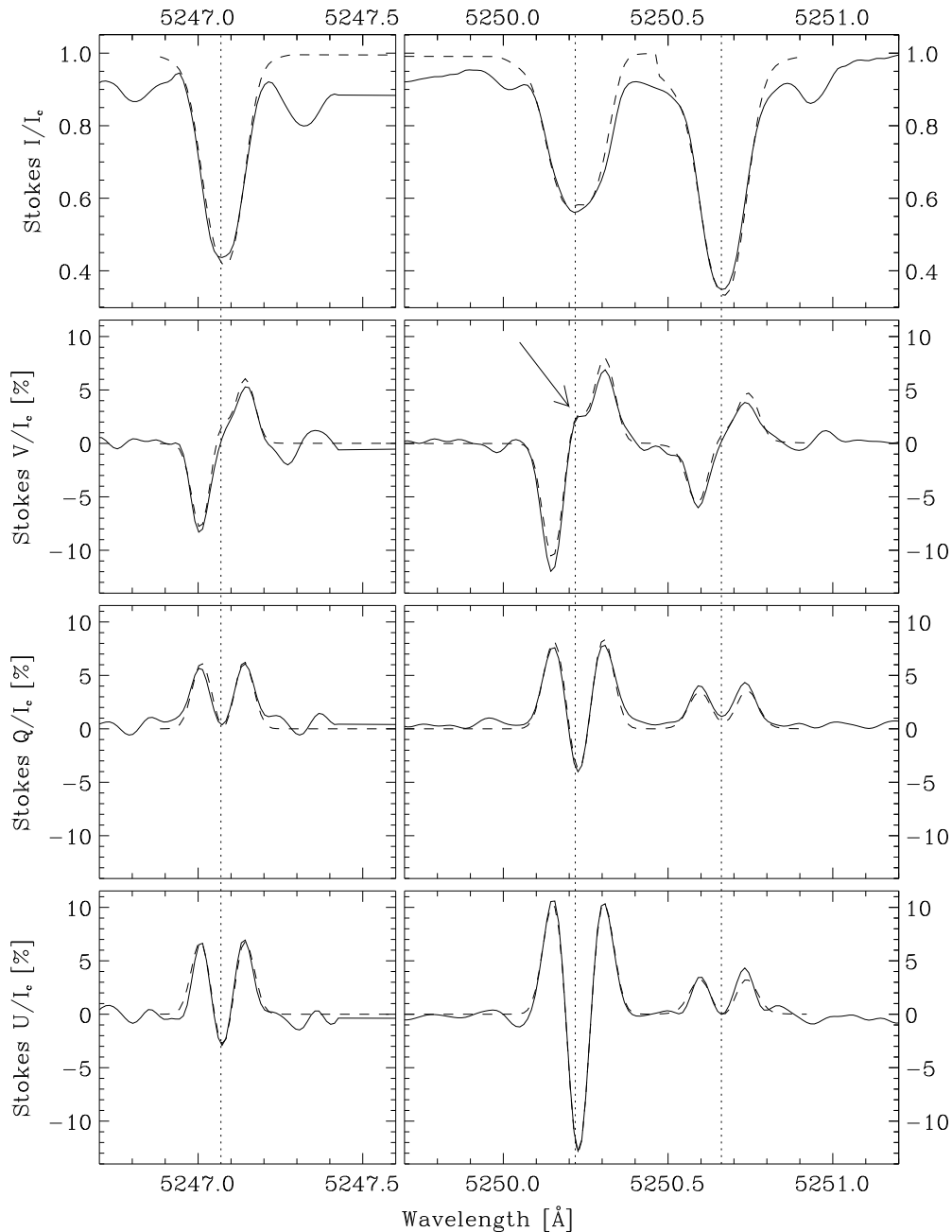


Fig. 5. Observed (solid) and synthetic (dashed) Stokes profiles for pixel position 21. The vertical dotted lines mark the wavelength of the Stokes I minima. The arrow marks the shoulder in the Stokes V profiles of Fe I 5250.2 Å that is discussed in the text.

Following Solanki et al. (1987) we have chosen a fixed value of 1.0 km s^{-1} for the microturbulent Doppler broadening ξ_{mic} in magnetic and non-magnetic components.

To calibrate the zero-level Doppler shift that is needed to correctly determine the LOS velocity we have inverted the Stokes I profiles for the quiet sun region at pixel positions 0 to 2, where we do not have any signal in the polarized Stokes profiles. The Doppler shifts obtained are then subtracted from the Doppler shifts resulting from the inversion of the profiles at the other pixel locations. The estimated 1σ error for the zero-level Doppler shift is 2 mÅ , which corresponds to an error of 0.1 km s^{-1} .

The dashed lines in Figs. 4 to 7 show the best fits to the measured Stokes profiles. Even the highly distorted shapes of the Stokes V profiles in Fig. 4 are reasonably well reproduced. To test the assumption that these spectra result from the superposition of profiles coming from two different magnetic atmospheres, we have tried to fit some of them by just considering one magnetic component and a combination of strong velocity and field-strength gradients along the LOS. All our attempts with such a model atmosphere failed (see Paper I). Only by considering model atmospheres with two magnetic components having different field strengths, field geometries, and velocity fields could we obtain good matches between synthetic and observed profiles. Note also the good agreement between synthetic and

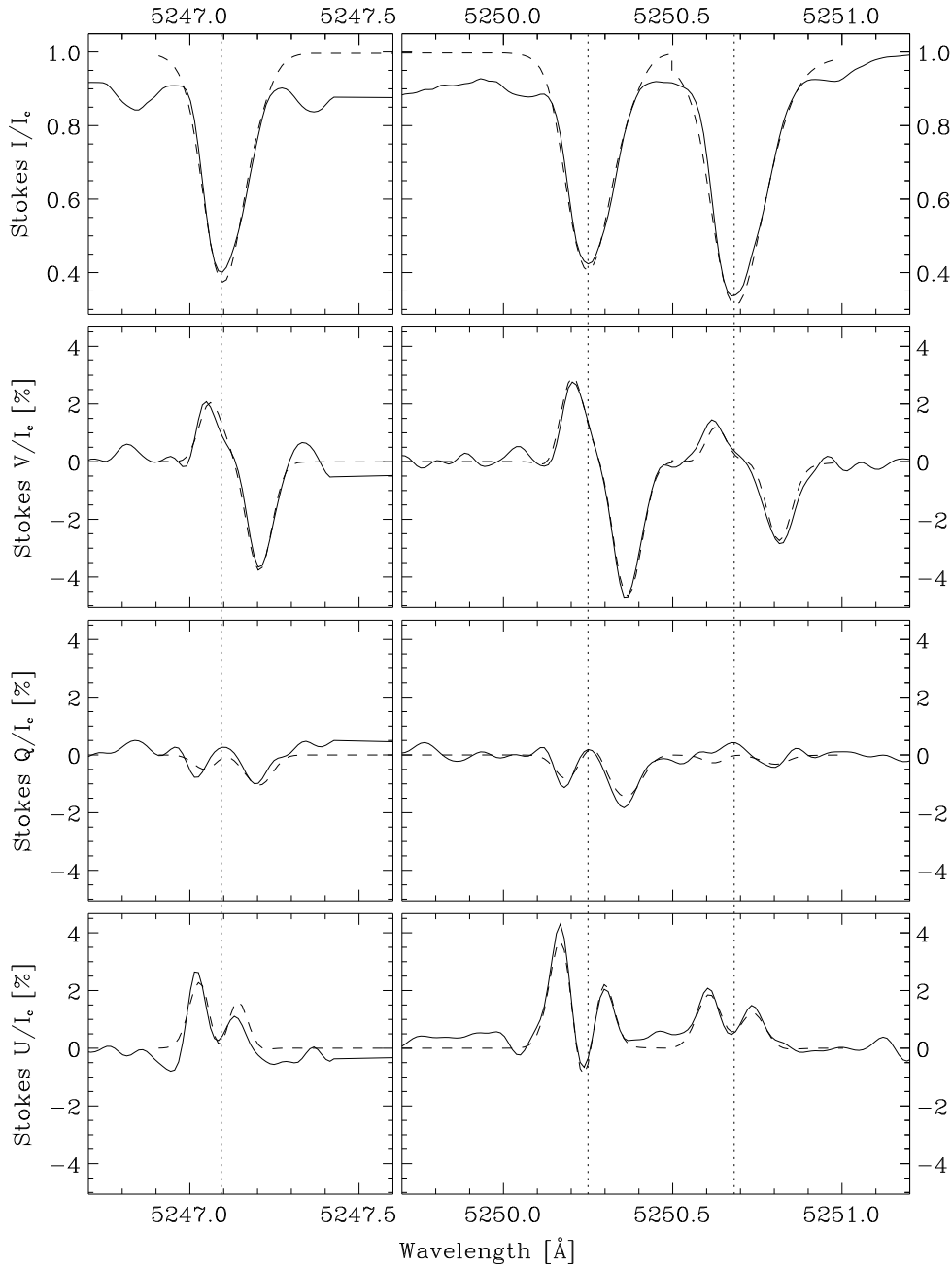


Fig. 6. Observed (solid) and synthetic (dashed) Stokes profiles for pixel position 43. The vertical dotted lines mark the wavelength of the Stokes I minima.

measured Stokes I profiles, even though we have assigned to them a weight ten times smaller than that of the polarization profiles.

Despite the good fits to the observed Stokes profiles, we caution that before achieving a good result, the inversion must be repeated several times, in particular when multiple magnetic components are present. In such cases the χ^2 hyper-surface that is minimized can have several local minima and the fit procedure might remain stuck in one of them. Therefore, the starting point on the χ^2 hyper-surface must be chosen as close as possible to the global minimum. To obtain a feeling for the sensitivity of the solutions to the initial values of the free parameters, we have run the inversion procedure several times with different initial

values. One method of ensuring rapid convergence is to use the atmospheric parameters that result from fits to the neighboring points. But sometimes the difference between the Stokes profiles of two adjacent spatial points is so large that this method does not work either. For the most complex Stokes profiles, such as those in Fig. 4, we repeat the inversion with many different guesses for the initial parameters until the correct set is found, so that the code just performs the final “tuning” of the output parameters.

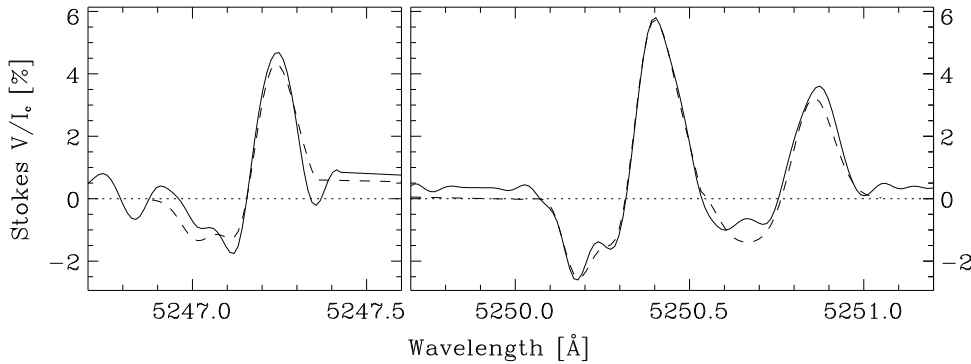


Fig. 7. Observed (solid) and synthetic (dashed) Stokes V profiles for pixel position 59. The anomalous shape of the profiles as well as the large area asymmetry can only be reproduced with a model atmosphere with two magnetic components in combination with velocity and magnetic field gradients along the LOS.

2.3. Transformation from the LOS to a local reference system

The magnetic field geometry returned by the inversion is in the LOS coordinate system. We then transform the inclinations and azimuths into the local heliographic coordinate frame, which has the z direction normal to the solar surface in the observed region. The x -axis is oriented parallel to the local heliographic $E - W$ direction, while the y -axis is parallel to the $N - S$ direction. The field direction in the local reference frame is given by the field inclination γ_l between the magnetic field lines and the solar vertical, and the local azimuth χ_l , which is counted counterclockwise from the heliographic W direction.

Because of the 180° ambiguity in the determination of the LOS field azimuths χ due to the symmetry properties of the transverse Zeeman effect, there are two possible orientations of the field lines in the local reference frame for each pixel position. Since we have observed the region at an angle θ of about 40° , not only will the azimuths χ_l of the two possible field orientations be different but also the inclinations γ_l . We thus need to choose between two possible field geometries, which may be very different. In the case of an inversion with two magnetic components, the choice must be done between four possible combinations, two for each magnetic component. The determination of the correct solution is not easy because we have only data at a single slit position, and we do not have any information about the geometry of the magnetic fields to the side of the slit. This precludes the use of algorithms based on the divergence-free method (e.g. Metcalf 1994; Li et al. 1993), which need a two-dimensional grid of points to solve the problem. Furthermore, since the observed active region shows a very complex magnetic structure, the simple assumption adopted by Bernasconi et al. (1995) that the correct solution should be the one that exhibits the smallest inclination to the solar normal is also no longer valid. Only in some cases can we make this simple assumption (e.g. in the small plage between pixel positions 80 and 100). In this case the buoyancy forces due to the partial evacuation of the flux tubes (Schüssler 1986) should prevail over other forces, so that we expect the flux tubes to be not too strongly inclined. In other cases we could make a choice by demanding consistency with other data. For example, the two spot-like structures visible in the lower part of the white-light image in Fig. 3 (to the east of the slit) have negative polarity. It is therefore most likely that the flux tubes between

pixel positions 10 and 45 also have negative polarity. One of the two possible solutions for the strongest magnetic component for those pixel positions has positive polarity (see Sect. 3.1), so it can be eliminated. Once we find a good solution for some pixel positions, we can use it to decide which is the correct solution for the adjacent pixel by assuming some degree of continuity between nearby positions. Although for many pixel positions it appears evident which solution should be the correct one, there are still some cases for which the ambiguity cannot be clearly resolved, sometimes because both solutions appear correct, and sometimes because none of them seems to be the correct one. In those cases we have chosen the solution that makes most sense in terms of the global structure of the whole active region.

In Fig. 8 we present the inferred field orientations projected onto the white-light image. They are also shown in Fig. 9, but in a 3-D representation. The length of the arrows in Fig. 8 is proportional to $\alpha B \sin \gamma_l$, while in Fig. 9 they are proportional to αB , which gives a better idea of the magnetic field structure. Fields with positive polarity are represented by arrows pointing away from the slit, and vice versa for fields with negative polarity. The white arrows represent the main magnetic component, while the dark or gray arrows represent the secondary magnetic component (the main magnetic component is defined to be the component with larger magnetic flux). In the lower left corner of the white-light image, the local heliographic reference system is indicated. The dark arrow labeled \odot points in the direction of disk center, the white arrow in the LOS direction. The solid horizontal lines divide the region into four parts, each showing distinct and peculiar characteristics. The dashed lines mark further subdivisions that will be discussed below. These subdivisions are also shown in Fig. 3.

3. Results and discussion

3.1. Field structure in a region with penumbral characteristics

The first region to be discussed ranges from pixel positions 6 to 47. The slit crosses a magnetic region very similar to a small penumbra that protrudes out from the two small spots located to the east of the slit. The two dashed lines at pixel positions 17 and 34 in Fig. 8 mark the points where the slit crosses the “penumbral” boundary, as deduced from the slit-jaw images. Almost all

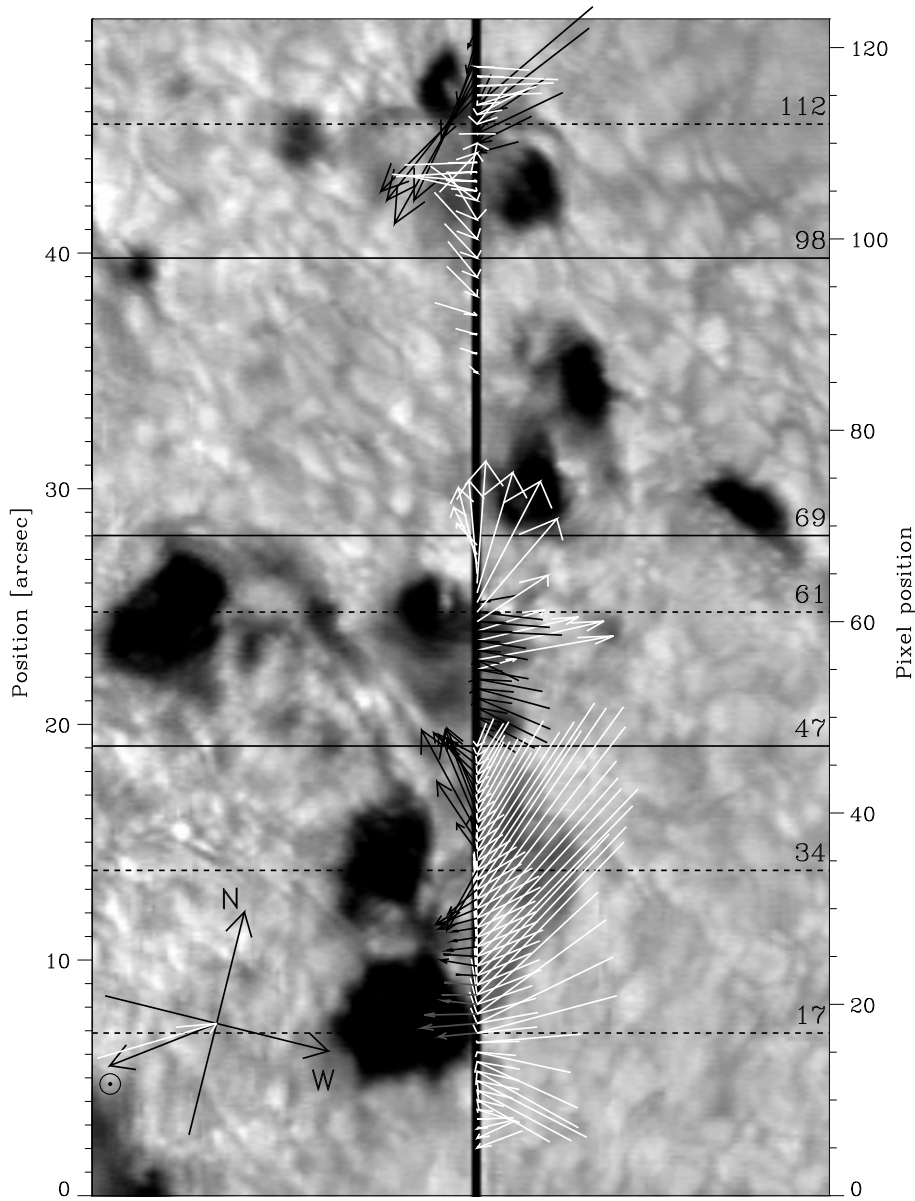


Fig. 8. Geometry of the field lines as seen from an observer placed above the active region. See the text in Sect. 2.3 for more details.

Stokes V profiles of the Fe I 5250.2 Å line in this region show a peculiar “shoulder” in the red wing (see Fig. 5).

Fig. 10 shows the temperature, field strength, and inclination of the field lines to the local solar vertical direction for pixel positions 6 to 47. The main magnetic component is represented by stars, while the secondary magnetic component is represented by diamonds. The “penumbral” boundaries are marked by the two vertical dashed lines that coincide with those depicted in Fig. 8. All values plotted in Fig. 10 refer to an optical depth of $\log \tau_{5000} = -1.5$ in the magnetic atmospheres. The estimated 1σ errors for the main component are 50 K for the temperature, 100 G for the field strength, and 4° for γ_l . The uncertainty in the determination of the parameters for the secondary magnetic component is considerably higher because its Stokes profiles are dominated by the main component, and the range of solutions producing similar synthetic profiles is larger. We estimate for

this component errors of the order of 100 K for the temperature, 150 G for the field strength, and 8° for γ_l .

Fig. 10 illustrates the difference between the two magnetic components in the “penumbra”. The field strength of the main component (white arrows in Fig. 8) ranges from 1300 to 1700 G with an average filling factor of 0.56 (not shown in the plot), the mean temperature lies around 4900 K, and the average field inclination is 40° . These fits were performed including the depth independent field gradient $\nabla B = \partial B / \partial \log \tau$ as a free parameter. Its average value is 450 G / $\log \tau$. These results are consistent with previous estimates of the inner part of penumbrae (Lites et al. 1990, 1993; Degenhardt & Wiehr 1991; Solanki et al. 1993; Keppens & Martínez Pillet 1996). The field lines of the second magnetic component are almost horizontal, and the field strengths are considerably weaker (840 G on average with a mean filling factor of 0.12), while the temperature is much

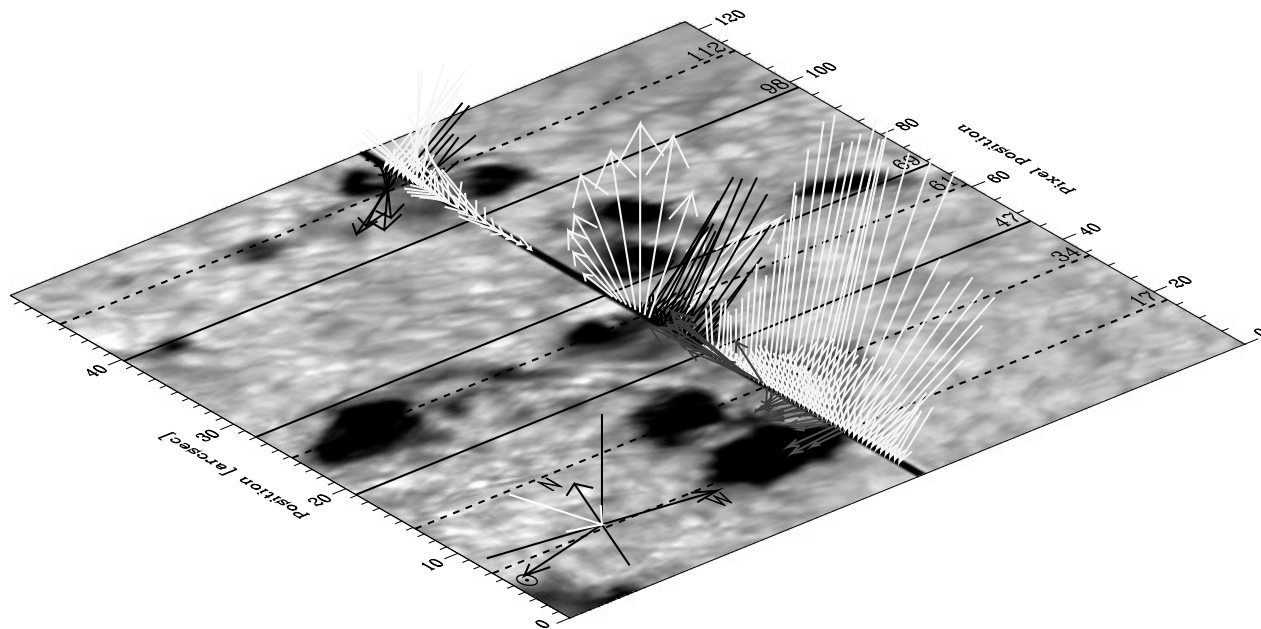


Fig. 9. Same as Fig. 8, but in a 3-D representation.

higher than in the main component (5400 K on average). The rest of the radiation is due to the non-magnetic components, presumably in the form of stray light from the non-magnetic surroundings.

The differences in Fig. 10 suggest that the two magnetic components do not just have different field orientations, but they also have very different physical properties. Furthermore, the Evershed flow derived from the Doppler shifts of the profiles of the Fe I 5250.2 Å line for both components confirms this hypothesis. The average line of sight velocity $\langle v_{LOS} \rangle$ for the main component is 0.5 km s^{-1} , while for the secondary component it is 2.7 km s^{-1} . With our observations we are not able to determine the actual direction of the velocity field vector, but if we assume that the gas streams parallel to the field lines, we can compute the field-aligned flow v_{FA} from

$$v_{FA} = v_{LOS} / \cos \gamma, \quad (2)$$

where γ is the angle between the LOS and the field lines. We obtain $\langle v_{FA} \rangle = 1.8 \text{ km s}^{-1}$ for the main component and $\langle v_{FA} \rangle = 3.2 \text{ km s}^{-1}$ for the secondary component. The Evershed flow is thus stronger in the horizontal component than in the main component.

From these results we draw the following picture: In the small penumbra-like structure there is a main magnetic component with field lines moderately inclined to the vertical, relatively strong field strength, some flow, and low temperature. A second magnetic component is embedded with the main component, and it has a weak, nearly horizontal field, high temperature, and strong outward flows. Golovko (1974) has proposed a similar model by interpreting the crossover effect in penumbrae (Babcock 1951; Grigorjev & Katz 1972) in terms of a superposition of radiation coming from different

elements of unresolved penumbral fine structures having opposite field polarity and different mass flows. More recently Parker (1992), Wentzel (1992), Solanki & Montavon (1993), and Schlichenmaier (private communication) have also proposed similar models. Wentzel has suggested that an upwelling at the footpoints of inclined flux tubes produces an instability that causes the flux tube to fall and stagnate horizontally some 100 km below the photosphere. Our observations indicate that the horizontal field should lie higher in the photosphere, since the spectral lines that we use are formed some 250 km above the continuum level of a penumbra ($\tau_{5000} = 1$) (Bruls et al. 1991), which means that we should not be able to see the fields if they lie as deep as proposed by Wentzel. On the other hand, according to Schlichenmaier et al., who model the convective rise of small flux tubes through the deep penumbra, the rising field comes to rest as horizontal tubes somewhat above $\tau = 1$, in agreement with our results. We confirm earlier conclusions that the Evershed flow mainly occurs in the regions with horizontal magnetic fields (Degenhardt & Wiehr 1991; Title et al. 1993; Hofmann et al. 1994; Rimmele 1995). Furthermore, Degenhardt & Wiehr (1991) and Hofmann et al. (1994) have found a certain degree of correlation between field strength and inclination, such that the horizontal flux tubes seem to have a weaker field than less inclined flux tubes. This agrees with our finding that the second, nearly horizontal component has a considerably lower field strength compared with the main component.

Our observations show that the temperature in the horizontal flux tubes is considerably higher than in the surrounding main penumbral magnetic component. This seems to be in contradiction with recent results derived from observations of infrared Ti I lines in sunspot penumbrae performed by Rüedi (1996). Rüedi also found the presence of weak horizontal fields in penum-

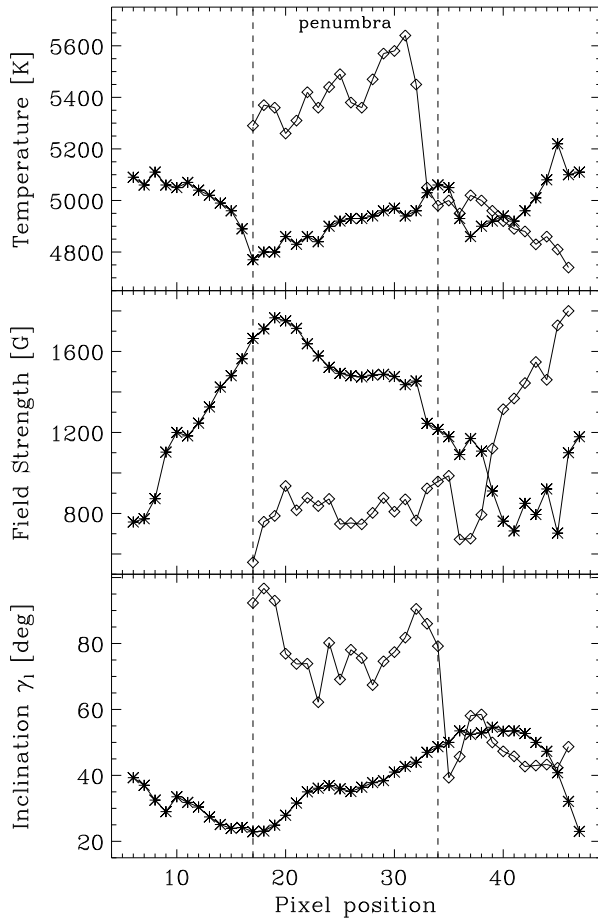


Fig. 10. Temperature T , field strength B , and field inclination γ_l vs. pixel position along the slit for pixels 6 to 47. The main component is labeled with stars, while diamonds represent the second component.

brae, but with considerably lower temperatures than we have found, since the Ti I lines form primarily in cold structures like e.g. in penumbrae (Rüedi et al. 1995). To check if this discrepancy is due to an incorrect estimate of the temperatures in our secondary component, which contributes little to Stokes profiles and, consequently, is not so well determined, we have performed test fits for some of the positions between pixels 17 and 34 by coupling the temperature in the two magnetic components, i.e., keeping the temperature as a free parameter, but forcing it to have the same values for both components. The inferred temperatures are about 5000 K, which is slightly higher than the temperatures originally found for the main magnetic component. The resulting synthetic Stokes V , Q , and U profiles are almost identical to the profiles resulting from the inversion with uncoupled temperatures. The most important difference occurs for the Stokes I profiles. While the synthetic Stokes I profiles obtained for the fit with uncoupled temperatures reproduce the observed profiles very well, the new synthetic Stokes I profiles are stronger, in particular in the red portion of the line core, which is affected most by the secondary magnetic component. Consequently the χ^2 values are higher for these test fits, so the

results are worse than those of fits with uncoupled temperatures. Although the temperature estimate for the secondary magnetic component is not so accurate, we still conclude that this component really possesses a temperature that is higher than that of the main component. We believe that the discrepancy with Rüedi's results may be due to the circumstance that what we observe is not a real sunspot penumbra, even if many characteristics are very similar, and it may possess some peculiar characteristics (e.g. hotter horizontal fields) that do not appear in "normal" penumbrae.

The two scatter plots in Fig. 11 show a clear relationship between B , T , and the field inclination γ_l at $\log \tau_{5000} = -1.5$ for the penumbral region (pixels 17 to 34). Flux tubes with a larger inclination to the vertical have higher temperatures and smaller field strengths. The main component (stars) shows a well defined behavior with little scatter compared with the points for the second component (diamonds), which scatter around the mean values $\gamma_l = 75^\circ$, $B = 850$ G, and $T = 5500$ K. The larger scatter of the values of the secondary component is mainly due to the circumstance that this component is not as well determined as the main component. Very similar relations have previously been found by Kopp & Rabin (1992) and Solanki et al. (1993) by analyzing $1.56 \mu\text{m}$ spectra in sunspots. It is interesting to note that their data refer to the optical depth $\log \tau_{16000} = 0$ that corresponds to deeper and hotter layers than the optical depth to which we refer (i.e. $\log \tau_{5000} = -1.5$). Thus the previously observed relations between γ_l , B , and T are also valid for higher and cooler photospheric layers. We must, however, stress that one should be very careful when comparing and interpreting relationships that refer to large spatial scales (like those of Kopp & Rabin and Solanki et al.) with relationships for small spatial scales (like ours), because they are not necessarily the same.

Around pixel position 34, there is a sudden change in the parameters for the second magnetic component (see Fig. 10). The temperature drops abruptly and levels out at values close to those of the main component, while the field strength increases rapidly and reaches the typical values for plage flux tubes (Solanki 1986; Keller et al. 1990; Bernasconi et al. 1995). γ_l also changes abruptly and drops from 80° to 40° . The most important change in the main component is the decrease of the field strength. The filling factor decreases gradually, and the flux becomes smaller than the flux of the former secondary component, so that the component that we previously defined as the main component no longer dominates the Stokes profiles and the roles of the two components are reversed. We feel that at this position the light from the outer edge of the penumbra mixes with another magnetic component that probably belongs to a plage that surrounds the whole active region. Of course, the transition from the weak penumbral component to the plage component is gradual, and at the boundary around pixel position 34 we should have at least three superimposed magnetic components. This is consistent with the circumstance that the three parameters shown in Fig. 10 do not change simultaneously, which suggests that the inversion results for the secondary component at these positions represent a mixture of two magnetic components.

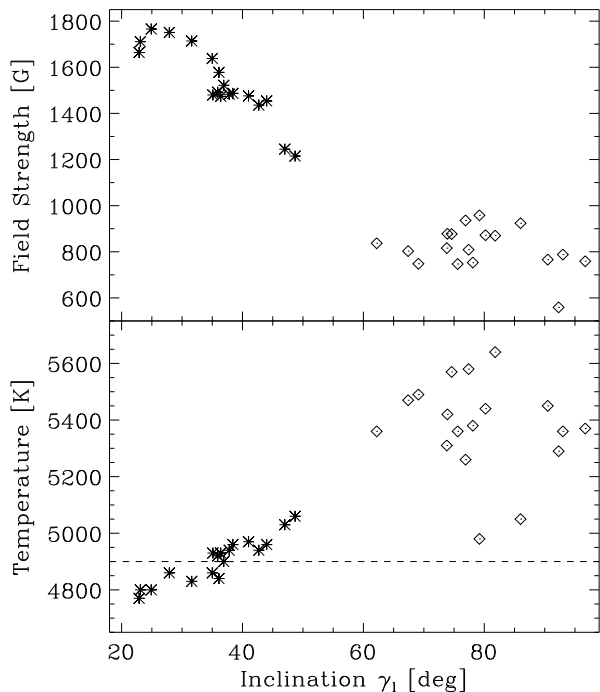


Fig. 11. Field strength vs. γ_l (top panel) and temperature at $\log \tau_{5000} = -1.5$ vs. γ_l (bottom panel) for the penumbra between pixel positions 17 and 34. The horizontal dashed line in the bottom panel marks $T(\log \tau_{5000} = -1.5)$ for the quiet-sun model of Maltby et al. 1986. Stars refer to the strong main magnetic component, while the weak, nearly horizontal component is labeled by diamonds.

3.2. Large downflows in a bipolar region

The second region that we discuss ranges from pixel positions 49 to 68. The slit first crosses a region with fields of negative polarity that appears rather dark in the continuum images, then it passes close to a pore with probably positive magnetic polarity (see slit-jaw image in Fig. 3). The results of the inversion are illustrated in Fig. 12. The negative polarity component (diamonds in Fig. 12 and black arrows in Figs. 8 and 9) possesses a rather low temperature and a magnetic field that is only slightly inclined to the vertical ($\sim 20^\circ$), with a field strength of around 1000 G. The Stokes profiles appear highly redshifted, which suggests the presence of a strong downflow inside the magnetic field component (see discussion below).

After pixel position 55 we start to see Stokes Q profiles that are considerably less redshifted with respect to the Stokes V profiles (compare the Q and V profiles in Fig. 3). This is similar to category 3 described in Sect. 2.1, i.e. we begin to see a second magnetic component with a smaller gas velocity and field lines nearly perpendicular to the LOS. Our results show that this component has a positive magnetic polarity (stars in Fig. 12 and white arrows in Figs. 8 and 9), and its field strength and temperature are higher compared with the other component. In Fig. 8 we see how the field lines change their direction gradually. They are probably influenced by the nearby pore. From position 61 onwards there is a Stokes V signal clearly belonging

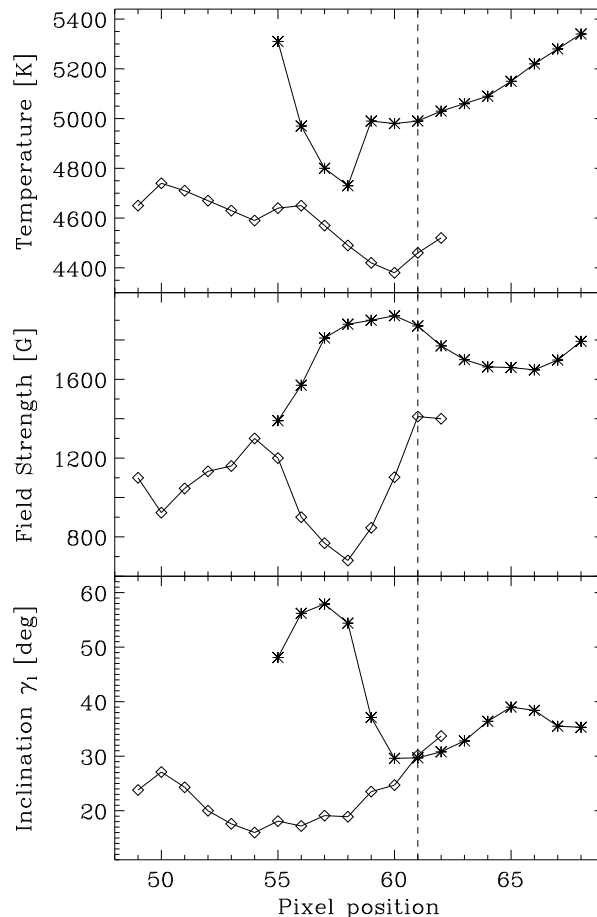


Fig. 12. Temperature, field strength, and field inclination vs. pixel position along the slit for pixels 49 to 68. The magnetic component with negative polarity is labeled by diamonds, while stars label the component with positive polarity. The vertical dashed line marks the neutral line observed in the Stokes V profiles (see also Fig. 3).

to this component as the flux tubes become less perpendicular to the LOS. Meanwhile, the Stokes profiles of the negative magnetic component gradually get smaller and disappear as its filling factor decreases. Possibly the positive magnetic component still belongs to the pore immediately eastward of the slit, which we suppose has positive polarity (unfortunately we do not see the magnetic signature of this pore on the Kitt Peak magnetogram in Fig. 1), even though the temperatures are higher and more similar to plage temperatures (Solanki 1986; Keller et al. 1990; Bernasconi et al. 1995). The opposite polarities of the two magnetic components suggest that the dark feature crossing the slit between pixels 48 and 66 is not a penumbra-like structure protruding from the pore just eastwards of the slit near pixel position 60, but is a separate magnetic feature.

As mentioned above, the Stokes profiles of the negative component appear to be strongly redshifted. From the shifts of the Fe I 5250.2 Å line found by the inversion code for this magnetic component we derive the velocities that are displayed in the bottom panel of Fig. 13. Stars represent the LOS velocities,

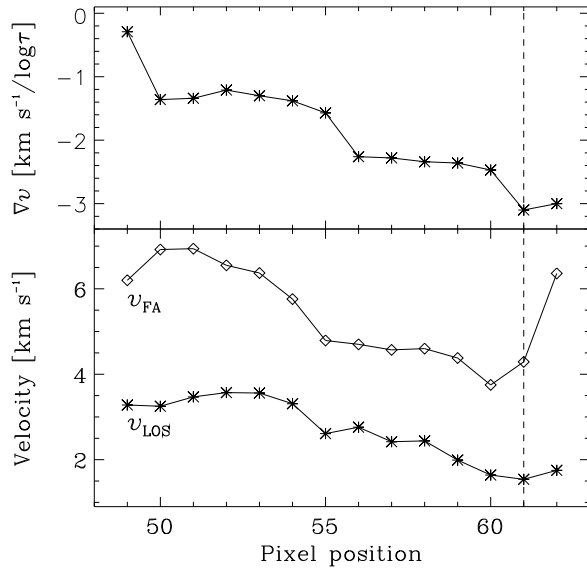


Fig. 13. LOS velocity gradients (top panel), LOS velocities at $\log \tau_{5000}$ (stars in bottom panel) and the corresponding field-aligned flow (diamonds in bottom panel) of the negative polarity region between pixel positions 49 and 62, derived from the fit results referring to the line Fe I 5250.2 Å.

while the diamonds are the corresponding field-aligned flows computed with Eq. 2. The estimated field-aligned downflow is remarkably large, reaching almost 7 km s^{-1} . From the gas pressure and gas density at $\log \tau = -1.5$ we estimate a sound speed of $6.5 \pm 0.5 \text{ km s}^{-1}$ for this magnetic component. Thus the maximum field-aligned velocities may be supersonic. Similar downflows have previously been observed by Martínez Pillet et al. (1994) at the neutral line of a δ -spot. Still, there are considerable differences. Firstly, Martínez Pillet et al. estimated a velocity of about 14 km s^{-1} , which is twice the maximum field-aligned downflow that we derive. Secondly, the maximum downflow value is not reached at the neutral line, but about $4''$ away from it, then v_{FA} gradually decreases while approaching the neutral line, where its value levels out at $\sim 4 \text{ km s}^{-1}$. These differences are probably due to the circumstance that we are not observing the same type of structure. While the downflowing region detected by Martínez Pillet et al. was very narrow (only $2''$ in diameter) and located inside the penumbra of a δ spot, the downflow that we observe extends over a larger area (about $5''$) and is located close to a pore of opposite magnetic polarity inside a complex group of pores.

The negative component not only shows a strong redshift, but also highly asymmetric Stokes profiles, in particular Stokes V (e.g. the Stokes V profiles for pixel position 59 displayed in Fig. 7). The blue wing is very small or almost nonexistent, while the red wing appears huge and broad. Note the bump at the center of the blue wing that suggests the presence of a second magnetic component. As explained in Sect. 2.2, to reproduce these abnormal Stokes profiles we must introduce a LOS velocity gradient ∇v in our model. The velocity gradients

determined by the inversion code for the first magnetic component are shown in the top panel of Fig. 13, where the dimension of ∇v is km s^{-1} per $\log \tau$. Since the $\log \tau$ scale increases with increasing geometrical distance from the observer, a negative gradient in our units means a slower gas flow deep in the solar atmosphere than in higher atmospheric layers.

When comparing the two panels in Fig. 13, we notice a strong anti-correlation between the velocities and the velocity gradient. Southward of pixel position 55, the gas streams with nearly supersonic velocity but is only moderately decelerated by the denser, deep-lying atmospheric layers (no exceptionally high velocity gradients in the line-forming layers). Around pixel position 55 we note a jump in both velocities and gradients. Northwards of this position the downflow becomes subsonic, while the absolute value of ∇v increases and reaches very high values, up to $-3.1 \text{ km s}^{-1} / \log \tau$. This anti-correlation might be explained by the presence of a shock front with variable height at different pixel positions. The supersonic, down-streaming gas is braked by hitting the denser, lower lying layers, and a shock front forms.

At least in the cases of siphon flows, the height of formation of the shock front depends on the pressure at the footpoint of the downflowing region (Thomas & Montesinos 1991). A higher pressure in the lower photospheric layers raises the shock-front height. It is possible that at around position 50, the shock front produced by the down-streaming gas is located slightly below the height of formation of our spectral lines, which is about 250 km above the continuum (Bruls et al. 1991), so that the gas in the observed layers is not so strongly braked and still has a high velocity. After pixel position 55, the shock front has moved above the height of formation of the lines. There the gas has lost most of its velocity and has become sub-sonic, while the large gradient suggests that it is still streaming supersonically at only a slightly greater height. To verify this hypothesis, we have compared the gas pressures at $\log \tau = 0$ in the model atmospheres provided by the inversion code for the best fits to pixel positions 52 and 58. The gas pressure for the second position was about 5 % higher than for the first position. This pressure difference appears quite small, but according to the calculations performed by Thomas & Montesinos (1991), a pressure increase of a few percent can raise the height of the shock front considerably. Thus all our data appear to be consistent with this interpretation. Nevertheless, it is not clear what physical mechanism produces such a strong downflow. What we see could, but need not, be the down-stream footpoint of a siphon flow in an arched flux tube. In any case we exclude the possibility that the nearby positive magnetic component is the corresponding up-stream footpoint of the siphon flow because the flux tubes of the second component also show a downflow with low gas velocities, $v_{LOS} = 0.4 \text{ km s}^{-1}$ on average, which corresponds to a v_{FA} of 0.9 km s^{-1} .

3.3. Weak plage

Between pixel positions 69 and 97, the Stokes profiles have small amplitudes. Only Stokes V profiles can be seen, while

the Stokes Q and U signals are buried in the noise, which may suggest that the field lines are nearly parallel to the LOS. For these profiles we have used an atmospheric model with a single magnetic component. The inversion code had considerable difficulties in finding the correct combination of field strength and filling factor. For most of the pixel positions, the code found values for B on the order of 300 G or smaller, which are too small compared to the field strength usually found in plages (e.g. Keller 1992 and references therein; Solanki 1993; Bernasconi et al. 1995; Martínez Pillet et al. 1997). On the other hand, the values for the filling factor α appear to be much too high ($\sim 35\%$ of the resolution element covered by the magnetic element). The inferred gas temperature of 5100 K on average is, however, consistent with what we would expect for plage flux tubes (cf. Keller et al. 1990; Bernasconi et al. 1995). We have repeated the inversions for the same profiles but kept B fixed at 800 G. The resulting synthetic Stokes I and V profiles also reproduced the observed profiles very well. The most important difference in the output parameters was a smaller value for α (now $\sim 15\%$), which was needed to compensate for the higher field strength. This means that the inversion code is not able to distinguish between a weak field strength with a high filling factor and a strong field strength with a small filling factor. Nevertheless, we can constrain the effective field strength value by computing the magnetic line ratio: $V_{5250.2}/(1.5 V_{5247.1})$ (Stenflo 1973; Stenflo & Harvey 1985), which allows us to set an upper limit to the field strength of about 900 G.

In this region the linear polarization is practically nonexistent, so it is difficult to correctly determine the field inclinations. In the weak-field regime, as in this case, Stokes V is proportional to B while Stokes Q and U are proportional to B^2 , which implies that Q and U are much smaller than V . Stokes Q and U are also proportional to $\sin^2\gamma$, which further contributes to reduce the amplitude of the linear polarization signals so that they become dominated by the noise. Our relatively high rms noise ($\sim 0.25\%$) only allows us to say that $\gamma \lesssim 30^\circ$, which means that $10^\circ \lesssim \gamma_l \lesssim 70^\circ$ (recall that $\theta = 40^\circ$).

3.4. Two pores with the same polarity?

The last region between pixel positions 98 and 122 is the most difficult to interpret. The slit passes between two pores that seem to be connected with a strange, penumbra-like structure. Starting from position 109, we see clear evidence of the presence of at least two magnetic components, but because of the complexity of the Stokes profiles, it is difficult to determine a unique set of parameters that would result in acceptable fits between synthetic and measured profiles.

Despite the great difficulties encountered in inverting these Stokes profiles, we are quite confident that our results are correct, because the range of possible values of the starting parameters that lead to a good fit is very narrow, and if the initial values are not correctly chosen, then no acceptable fit to the observations is found. Hence, although there appear to be multiple minima in the χ^2 hypersurface, the global minimum is much deeper than the rest.

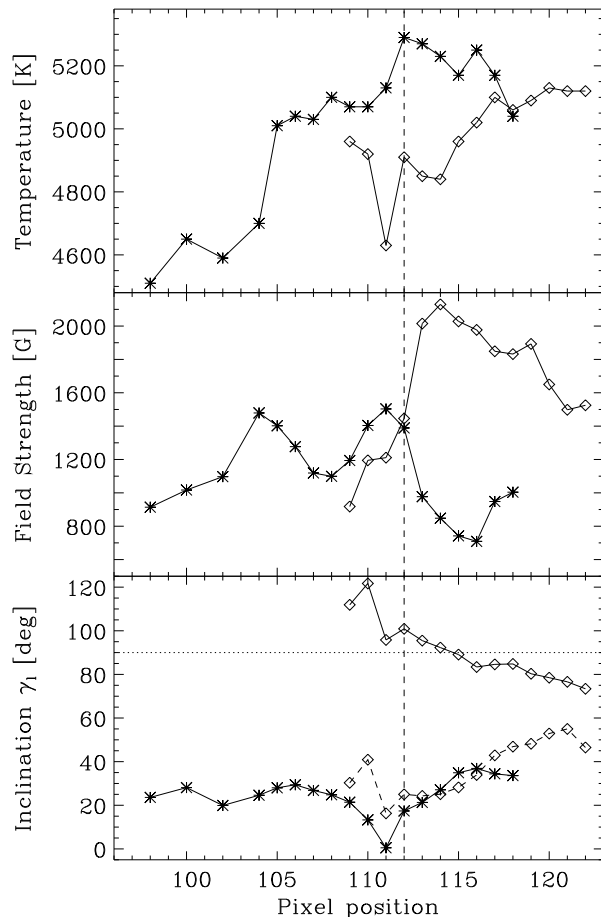


Fig. 14. Temperature, field strength, and field inclination vs. pixel position for pixels 98 to 122 along the slit. Stars indicate the results for component 1 and diamonds for component 2. The diamonds connected with a dashed line in the bottom panel represent the second solution for component 2 (see text for more details). The vertical dashed line marks the neutral line observed in the Stokes V profiles (see Fig. 3). The horizontal dotted line indicates the horizontal field direction, i.e. $\gamma_l = 90^\circ$. Values of γ_l larger than 90° represent negative polarity fields.

The next problem we have encountered consisted in finding the correct solution for the 180° ambiguity for one of the two components. While for component 1 (white arrows in Figs. 8, 9, and 15 and stars in Fig. 14) it was quite clear which the correct solution was, for component 2 (black arrows in Figs. 8, 9, and 15 and diamonds in Fig. 14) both solutions are physically acceptable. In the bottom panel of Fig. 14 we show both possible solutions for γ_l . For clarity in Fig. 8 only one solution for the field direction is shown. We believe that this is likely to be the correct solution (see below). The corresponding field inclinations in Fig. 14 are displayed with diamonds connected by a solid line. The longitudinal component for the other solution is displayed in Fig. 15, and the corresponding inclinations are the diamonds connected by a dashed line in Fig. 14.

When inspecting the field geometry of component 1, we note that the field first points away from the pore located to the right of the slit (pore 1) and its inclination remains constant at

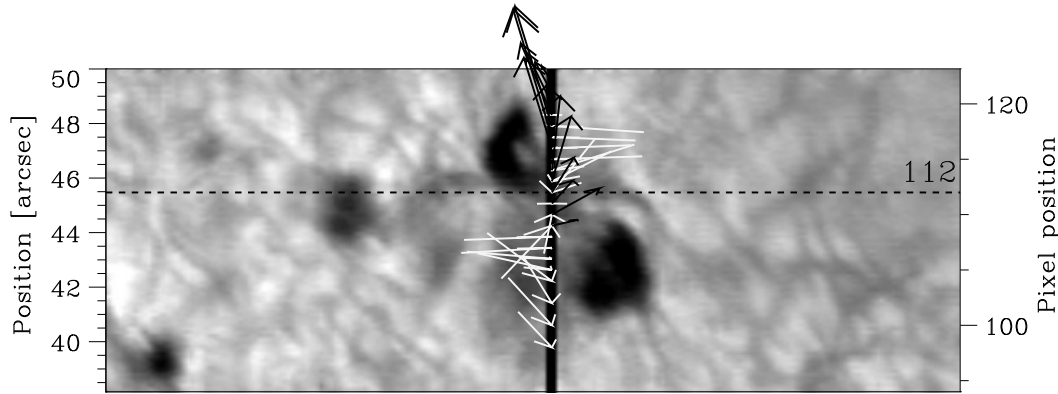


Fig. 15. Same as in Fig. 8 from pixel position 98 to 122. The black arrows show the field direction for the second solution for component 2. The dashed line marks the neutral line position observed in the Stokes V profiles.

about 20° , then as we move towards the second pore (pore 2), the field changes its azimuthal orientation slowly but constantly while its inclination decreases. At pixel position 111, which almost corresponds to the neutral line observed in the Stokes V profiles, the field lines are nearly vertical. After this point, the inclination increases again and the field lines now point towards pore 2. Note that the polarity remains negative for positions northward of the neutral line too. This magnetic structure suggests that both pores have the same negative polarity, and that the apparent neutral line in Stokes V is just due to a geometrical effect caused by the relatively large heliocentric angle under which we observe the region. If the observed fields do not point directly at the pores, but at a location about $2''$ outside their continuum boundaries, they still must belong to the same magnetic structure as the pores, since it extends several seconds of arc out from the pore boundaries that are observed in the continuum (Keppens & Martínez Pillet 1996). In fact, the inclinations and field strengths we derive are consistent with the values found by Keppens & Martínez Pillet at the outer magnetic boundary of pores.

It is not easy to verify whether pore 2 really possesses the same polarity as pore 1, since also the high-resolution Kitt Peak magnetogram (Fig. 1) can not provide a definitive answer.

The complexity of the field structure in this region is confirmed by the ambiguous results for the second magnetic component. One of the two possible solutions (solution 1: the diamonds that are connected by a solid line in the bottom panel of Fig. 14) shows nearly horizontal flux tubes first with negative polarity, after which the inclination gradually changes and the polarity becomes positive. We do not think that these are the same type of horizontal flux tubes that we saw in the penumbral structure discussed in Sec. 3.1, firstly because they are oriented almost perpendicular to a hypothetical line connecting the center of the two pores and not radially as would be expected for an undisturbed penumbra. Secondly, the inferred field strengths are much too high compared to the values that we have found for the horizontal fields in the penumbra. We believe that if this solution is the correct one, the particular field line orientation

in the second component may be due to the circumstance that both pores have the same polarity. At the plane of equal distance from the two pores, the field lines are bent due to their mutual magnetic repulsion and oriented parallel to this plane. Why the flux tubes are so horizontal is not clear either. It is likely that the fields with positive polarity close to pore 2 belong to a small plage where the magnetic field lines turn back forming small, closed loops. Indeed the values for field strength and temperature are similar to those of plages.

The other of the two physically acceptable solutions is even more puzzling. The fields have positive polarity. Close to the neutral line they stay relatively vertical, then the inclination gradually increases when moving northward. If we believe that this component belongs to pore 2, then it seems that this pore must have positive magnetic polarity, i.e. opposite with respect to pore 1, but the field lines are not oriented in the radial direction with respect to the pore center (see Fig. 15). On the other hand, if we accept the conclusion that this pore has negative polarity like pore 1 as inferred from the magnetic structure of component 1, then it has to be explained how flux tubes with positive magnetic polarity might exist inside a region with strong negative magnetic fields. In this case the second magnetic component would appear to be unrelated to either pore.

The mass motions inside this region are also intriguing. Component 1 shows Doppler velocities towards the observer on the order of 1 to 2 km s^{-1} across the whole region. Only for a few pixel positions at the neutral line does the flow vanish almost completely. In contrast, component 2 shows motions away from the observer, i.e. redshifts, of about 1 km s^{-1} . The observed flow for pixel positions from 98 to 112 seems to be similar to a normal Evershed flow, although the field lines are nearly vertical. On the other hand the blueshifts of component 1 for pixel positions 113 to 122 are hard to understand. Assuming an outflow from pore 2, we would expect a redshift. Only in component 2 do we see a redshift. If we assume that the two pores have the same polarity, which we do not know with certainty, we could exclude the possibility that pore 2 might be

the down-stream footpoint of a closed loop with pore 1 as the upstream footpoint.

Summarizing, we can say that this last region is very problematic because of its intricate magnetic structure. Our results do not fit the picture of a simple field around two pores, but an additional field component also appears to be present. Our multicomponent analysis reveals a high degree of complexity of small-scale magnetic structures which cannot be easily interpreted. It could also be that in this case our code is unable to correctly solve the inversion problem in its full complexity, even if the resulting synthetic profiles reproduce the observed Stokes profiles rather well. Maybe for this reason our results appear ambiguous and sometimes contradictory and difficult to interpret.

4. Conclusions

We have presented the results of a detailed analysis of measurements of the full Stokes vector in a complex active region based on an inversion of the Stokes profiles with a 3-component atmospheric model. This new approach was needed to reproduce the sometimes highly distorted Stokes profiles that cannot be easily understood in terms of a single magnetic component with velocity and field strength gradients in addition to a non-magnetic quiet Sun component. In some cases, when the Stokes V profiles look similar to linear polarization profiles, they can be reproduced in terms of two magnetic atmospheres with opposite polarities and different Doppler velocities. In other cases, the signatures revealing the presence of two magnetic components are more subtle, and measurements of the full Stokes vector are required to detect their presence. For example, when Stokes V and Q profiles of the same spectral line show different Doppler shifts, one component must have its magnetic field nearly parallel to the LOS while the other is perpendicular to it. In addition the mass motions in the two components must be different.

In the present work, we have attempted to reproduce complicated Stokes profiles with two magnetic and one field-free components along parallel lines of sight. The three model atmospheres are independent of each other. Variations of the magnetic field strength and mass flows along the line of sight are taken into account to first order by fitting the gradients of these two quantities. In general, the observed Stokes profiles will be affected by variations of the magnetic field vector and other atmospheric parameters along the line of sight and by the averaging over many parallel lines of sight due to the limited spatial resolution. Therefore, the three-component model used here is a rather simple model of reality, and the fitted atmospheres for the two magnetic components might not correspond to any particular structure in the observed region. Nevertheless, the three-component approach presents a major step towards a better understanding of magnetic field structures in complex active regions.

Our multi-component analysis has revealed the presence of two different magnetic components in a small region similar to a penumbra. Our observations thus support the widely accepted picture that the penumbral magnetic structure is composed of

two components. One component is much more inclined to the vertical, has lower field strengths, and shows larger outflows than the main component in which it is embedded. We are not able to confirm or refute the hypothesis that this component is associated with dark penumbral filaments.

Despite the high success rate of our code in inverting the observed Stokes profiles, excessive profile complexity may sometimes lead to unreliable results, as in the case of the region between pixel positions 98 and 122. There the inferred parameters, if correct, are difficult to interpret.

Inverting Stokes profiles with a 3-component model requires a large amount of computational time, the initial parameters must be set manually, and all resulting profiles must be checked visually to be sure that the code has found the lowest minimum of the χ^2 hyper-surface. At the present stage of the code development, we can only invert a limited number of Stokes profiles restricting us to the analysis of a single slit position. Nevertheless, we have demonstrated that to improve our understanding of complex magnetic structures, e.g. sunspot penumbrae, sophisticated multicomponent atmospheric models with depth dependent parameters are needed. For future inversions of a two-dimensional grid of spatial points, we should develop new strategies. A possible way will be a two-step inversion. First all the Stokes spectra over the whole region are inverted with a very simple 2-component model with a few free parameters. Then for the most interesting or most complex positions, the inversion is repeated with a more complex model, possibly with multiple magnetic components.

The most striking feature of the magnetic configurations that is revealed by our inversions is their complexity. Only at a minority of the spatial locations along the slit was a straightforward interpretation of all magnetic components possible in terms of our previous knowledge of simple plage and pore magnetic fields. Although the positioning of the slit (skirting 7 pores, with a total of 5 polarity inversion lines along its length) was a particularly complex part of the active region, our results nevertheless suggest that at least in some parts of active regions the results of models based on a single magnetic component must be considered with caution. We stress that magnetograph observations using only a few points in the line profiles will not reveal the presence of a second magnetic component. This component will, however, affect the magnetograph signal, so that major errors may result from an uncritical interpretation.

Acknowledgements. We are grateful to H.P. Povel, U. Egger, and P. Steiner for developing ZIMPOL I and for their invaluable technical support during the observations. We also thank F. Aebersold who constructed all mechanical parts. NSO/Kitt Peak data used here are produced cooperatively by NSF/NOAO, NASA/GSFC, and NOAA/SEL. This work was supported by the Swiss National Science Foundation, grant No. 20-37323.93, which is gratefully acknowledged. Finally, we wish to thank our referee, C. Bendlin, for careful reading of and commenting on the manuscript.

References

Auer, L.H., Heasley, J.N., 1978, A&A 64, 67

- Babcock, H.W., 1951, *ApJ* 114, 1
- Bernasconi, P.N., Keller, C.U., Povel, H.P., Stenflo, J.O., 1995, *A&A* 302, 533
- Bernasconi, P.N., Solanki, S.K., 1996, *Sol. Phys.* 164, 277 (Paper I)
- Bruls, J.H.M.J., Lites, B.W., Murphy, G.A., 1991, in *Solar Polarimetry*, L. November (Eds.), National Solar Obs., Sunspot, NM, p. 444
- Degenhardt, D., Wiehr, E., 1991, *A&A* 252, 821
- Golovko, A.A., 1974, *Sol. Phys.* 37, 113
- Grigorjev, V.M., Katz, I.M., 1972, *Sol. Phys.* 22, 119
- Hofmann, J., Deubner, F.-L., Fleck, B., Schmidt, W., 1994, *A&A* 284, 269
- Keller, C.U., 1992, Ph.D. Thesis, No. 9953, ETH, Zürich, p. 30
- Keller, C.U., Solanki, S.K., Steiner, O., Stenflo, J.O., 1990, *A&A* 233, 583
- Keller, C.U., Aebersold, F., Egger, U., et al., 1992, LEST Technical Report No. 53
- Keppens, R., Martínez Pillet, V., 1996, *A&A* 316, 229
- Kopp, G., Rabin, D., 1992 *Sol. Phys.* 141, 253
- Li, J., Cuperman, S., Semel, M., 1993, *A&A* 279, 214
- Lites, B.W., Scharmer, G.B., Skumanich, A., 1990, *ApJ* 355, 329
- Lites, B.W., Elmore, D.F., Seagraves, P., Skumanich, A., 1993, *ApJ* 418, 928
- Maltby, P., Avrett, E.H., Carlsson, M., et al., 1986, *ApJ* 306, 284
- Martínez Pillet, V., Lites, B.W., Skumanich, A., Degenhardt, D., 1994, *ApJ* 425, L113
- Martínez Pillet, V., Lites, B.W., Skumanich, A., 1997, *ApJ* 474, 810
- Metcalfe, T.R., 1994, *Sol. Phys.* 155, 235
- Parker, E.N., 1992, in *Sunspots: Theory and Observations*, J.H. Thomas, N.O. Weiss (Eds.), Kluwer, Dodrecht, p. 413
- Povel, H.P., 1995, *Optical Engineering* 34(7), 1870
- Povel, H.P., Aebersold, H., Stenflo, J.O., 1990, *Applied Optics* 29, 1186
- Povel, H.P., Keller, C.U., Yadigaroglu, I.-A., 1994, *Applied Optics* 33, 4254
- Press W.H., Flannery B.P., Teukolsky S.A., Vetterling V.T., 1990, in *Numerical Recipes. The Art of Scientific Computing*, Cambridge University Press, Cambridge
- Rimmele, T.R., 1995, *A&A* 298, 260
- Rüedi, I., 1996, Ph.D. Thesis, No. 11886, ETH, Zürich
- Rüedi, I., Solanki, S.K., Rabin, D., 1992a, *A&A* , 261, L21
- Rüedi, I., Solanki, S.K., Livingston, W., Stenflo J.O., 1992b, *A&A* 263, 323
- Rüedi, I., Solanki, S.K., Livingston, W., Harvey, J., 1995, *A&AS* 113, 91
- Schüssler, M., 1986, in *Small Scale Magnetic Flux Concentrations in the Solar Photosphere*, W. Deinzer, M. Knöllker, H.H. Voigt (Eds.), Vandenhoeck & Ruprecht, Göttingen, p. 103
- Skumanich, A., Lites, B.W., 1991, in *Solar Polarimetry*, L. November (Ed.), National Solar Observatory, Sunspot, NM, p. 307
- Solanki, S.K., 1986, *A&A* 168, 311
- Solanki, S.K., 1989, *A&A* 224, 225
- Solanki, S.K., 1993, *Space Sci. Rev.* 63, 1
- Solanki, S.K., Keller, C.U., Stenflo, J.O., 1987, *A&A* 188, 183
- Solanki, S.K., Rüedi, I., Livingston, W., 1992, *A&A* 263, 339
- Solanki, S.K., Montavon, C.A.P., 1993, *A&A* 175, 283
- Solanki, S.K., Walther, U., Livingston, W., 1993, *A&A* 277, 639
- Solanki, S.K., Montavon, C.A.P., Livingston, W., 1994, *A&A* 283, 221
- Stenflo, J.O., 1973, *Sol. Phys.* 32, 41
- Stenflo, J.O., 1991, LEST Technical Report No. 44
- Stenflo, J.O., Harvey, J.W., 1985, *Sol. Phys.* 95, 99
- Thomas, J.H., Montesinos, B., 1991, *ApJ* 375, 404
- Title, A.M., Frank, Z.A., Shine, R.A., Tarbell, T.D., Topka, K.P., 1993, *ApJ* 403, 780
- Wentzel, D.G., 1992, *ApJ* 388, 211